

See discussions, stats, and author profiles for this publication at: <https://www.researchgate.net/publication/280999000>

# Nd(3+)-Sensitized Ho(3+) Single-Band Red Upconversion Luminescence in Core-Shell Nanoarchitecture

ARTICLE *in* JOURNAL OF PHYSICAL CHEMISTRY LETTERS · JULY 2015

Impact Factor: 7.46 · DOI: 10.1021/acs.jpclett.5b01180 · Source: PubMed

---

CITATIONS

6

READS

64

## 6 AUTHORS, INCLUDING:



Daqin Chen

Hangzhou Dianzi University

165 PUBLICATIONS 3,399 CITATIONS

[SEE PROFILE](#)



Mingye Ding

Hangzhou Dianzi University

38 PUBLICATIONS 197 CITATIONS

[SEE PROFILE](#)



Jiasong Zhong

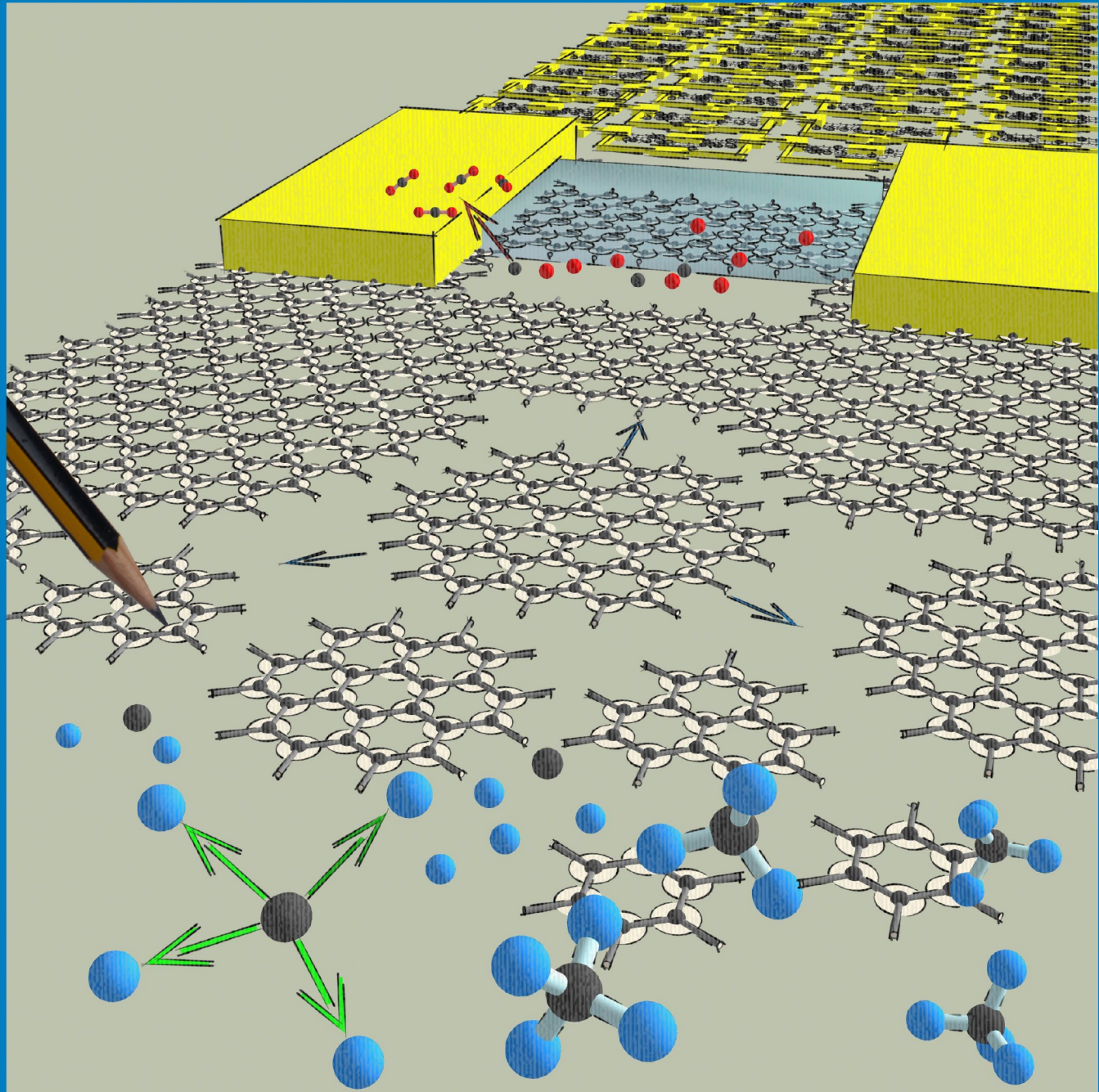
Tongji University

66 PUBLICATIONS 310 CITATIONS

[SEE PROFILE](#)

# THE JOURNAL OF PHYSICAL CHEMISTRY *L**e**t**t**e**r**s*

July 16, 2015 | Volume 6, Number 14



Drawing the 2D Roadmap: CVD Enabled Graphene Manufacture and Technology



ACS Publications  
Most Trusted. Most Cited. Most Read.

[www.acs.org](http://www.acs.org)

## Nd<sup>3+</sup>-Sensitized Ho<sup>3+</sup> Single-Band Red Upconversion Luminescence in Core–Shell Nanoarchitecture

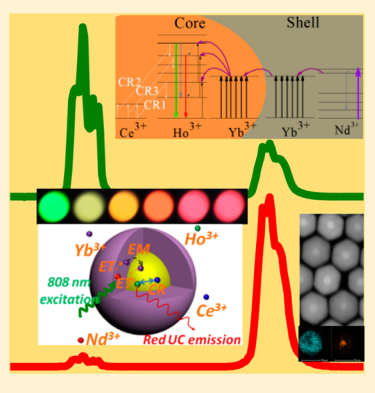
Daqin Chen,\*† Lu Liu,<sup>†</sup> Ping Huang,<sup>‡</sup> Mingye Ding,<sup>†</sup> Jiasong Zhong,<sup>†</sup> and Zhenguo Ji<sup>†</sup>

<sup>†</sup>College of Materials & Environmental Engineering, Hangzhou Dianzi University, Hangzhou 310018, P. R. China

<sup>‡</sup>State Key Laboratory of Structural Chemistry, Fujian Institute of Research on the Structure of Matter, Chinese Academy of Sciences, Fuzhou, Fujian 350002, P. R. China

### Supporting Information

**ABSTRACT:** A strategy to achieve 808 nm excited single-band red upconversion luminescence of Ho<sup>3+</sup> via the core–shell nanoarchitecture design was provided. Specifically, the synthesized Yb/Ho/Ce: NaGdF<sub>4</sub>@Yb/Nd: NaYF<sub>4</sub> active-core@active-shell nanoparticles were evidenced to enable high-content doping of Nd<sup>3+</sup> (~10 mol %) in the shell layer and, thus, markedly enhance red upconversion emission from Ho<sup>3+</sup> activators in the core with the assistance of spatially confined doping of Nd<sup>3+</sup> ions and efficient energy transfer of Nd<sup>3+</sup> → Yb<sup>3+</sup>(shell) → Yb<sup>3+</sup>(core) → Ho<sup>3+</sup>. Importantly, introducing Ce<sup>3+</sup> into the core was beneficial to the competition of radiation transitions from the two intermediate excited states of Ho<sup>3+</sup>: <sup>5</sup>S<sub>2</sub>, <sup>5</sup>F<sub>4</sub> (green-emitting) and Ho<sup>3+</sup>: <sup>5</sup>F<sub>5</sub> (red-emitting), which induced great enhancement in the red to green intensity ratio and ultimately intense single-band red upconversion emission. We believe that this preliminary study will provide an important advance in developing luminescent markers suitable for biolabeling applications.



Lanthanide (Ln<sup>3+</sup>) ion-doped upconversion (UC) nanoparticles (NPs) have been extensively investigated recently inspired by their potential applications as biomarkers, owing to their unique optical properties, such as sharp emission bands, long luminescent lifetimes (micro- to milliseconds), good photostability, and low background autofluorescence, as well as low toxicity.<sup>1–5</sup> UC is an anti-Stokes process where the low-energy photons are converted into a high-energy one via a two- or multiphoton absorption mechanism.<sup>6</sup> Generally, UCNPs were simultaneously doped with Yb<sup>3+</sup> as sensitizers and Er<sup>3+</sup>, Ho<sup>3+</sup>, or Tm<sup>3+</sup> as activators, where the input near-infrared (NIR) photons (~980 nm) were absorbed and then further transferred to the activators to yield ultraviolet, blue, green, red and NIR photons.<sup>7–12</sup> Unfortunately, the use of the 980 nm NIR photon as the excitation source has an intrinsic disadvantage since the water molecules in biological tissues exhibit a high absorbance at 980 nm.<sup>13</sup> As a consequence, the input 980 nm excitation light to trigger the UC process would be significantly attenuated and the absorbed light energy would lead to a risk of local temperature rise and even overheating of tissues under continuous irradiation.<sup>14,15</sup> Therefore, to make UCNPs more suitable for biological applications it is highly desirable to optimize the excitation light wavelength into an appropriate range. In fact, based on large absorption cross section around 800 nm of Nd<sup>3+</sup> (about 10 times of that of Yb<sup>3+</sup> at 980 nm) in conjunction with the efficient energy transfer (ET) from the excited Nd<sup>3+</sup> to Yb<sup>3+</sup>, intense UC luminescence can be easily realized under 800 nm laser excitation.<sup>14–20</sup> In such situation, Yb<sup>3+</sup> plays a role as the ET bridging ion between a donor (Nd<sup>3+</sup>) and an acceptor (Er<sup>3+</sup>, Ho<sup>3+</sup>, and Tm<sup>3+</sup>).

Importantly, the overheating effect could be largely alleviated because of the low 800 nm absorption coefficient for water molecules in biological tissues.

On the other hand, it is well known that Ln<sup>3+</sup> activators doped in the appropriate hosts generally have abundant metastable excited states, which enable them to emit photons covering from ultraviolet to infrared spectral region. Unfortunately, this kind of multiple-band spectral feature induces energy deconcentration and is disadvantage to achieving high-efficient UC luminescence for a specific Ln<sup>3+</sup> emitting state. Therefore, searching special UC hosts<sup>21–23</sup> or energy transfer routes<sup>24–27</sup> to achieve single-band and high-efficiency luminescence of Ln<sup>3+</sup> remains a formidable challenge but is highly desirable. Recently, several attempts have been made to obtain a high-purity, single-band UC red (~650 nm) emission of Ln<sup>3+</sup> doped NCs that is attractive for biolabels. Such dark red luminescence falls within the “optical window” of biotissues that could afford the deep tissue penetration. For instance, increasing Yb<sup>3+</sup> content in Yb<sup>3+</sup>/Er<sup>3+</sup>: NaYF<sub>4</sub> nanocrystals (NCs) was beneficial to the realization of high red-to-green emission ratio.<sup>10</sup> Introducing Ce<sup>3+</sup> into Yb<sup>3+</sup>/Ho<sup>3+</sup>: NaYF<sub>4</sub> or Na(Y<sub>0.6</sub>Gd<sub>0.4</sub>)F<sub>4</sub> NCs greatly enhanced red to green UC emission ratio of Ho<sup>3+</sup>,<sup>25,27</sup> doping Mn<sup>2+</sup> into Yb<sup>3+</sup>/Er<sup>3+</sup>: NaYF<sub>4</sub> NCs resulted in pure single-band red UC emission via efficient ET between Mn<sup>2+</sup> and Er<sup>3+</sup>,<sup>26</sup> special Na<sub>3</sub>Zr(Hf)F<sub>7</sub> host was designed to achieve intrinsic single-band red emission

Received: June 4, 2015

Accepted: July 2, 2015



for  $\text{Er}^{3+}$  activators owing to the formation of  $\text{Ln}^{3+}$  cluster in this medium.<sup>22</sup>

In the present work, we reported for the first time the realization of 808 nm excited single-band red UC luminescence of  $\text{Ho}^{3+}$  activators in a specially designed Yb/Ho/Ce:  $\text{NaGdF}_4@\text{Yb}/\text{Nd}: \text{NaYF}_4$  active-core@active-shell nanoarchitecture.  $\text{NaGdF}_4$  was chosen as core for its easy formation of hexagonal phase, and  $\text{NaYF}_4$  was adopted as shell in order to clearly discern core–shell structure for the large difference of atomic number between Y and Gd. The roles of  $\text{Ce}^{3+}$  ions in the core and  $\text{Nd}^{3+}$  ions in the shell as the assisted centers of cross-relaxation for red emission and the sensitizers for efficient absorption of 808 nm photons respectively were clearly clarified.  $\text{Yb}^{3+}$  ions acted as efficient energy migrators (or bridging centers) to facilitate energy transfer from  $\text{Nd}^{3+}$  sensitizers to activator ions (i.e.,  $\text{Ho}^{3+}$ ). Notably, the active-core@active-shell nanostructure was demonstrated to be necessary for the high-content  $\text{Nd}^{3+}$  doping to greatly enhance red UC luminescence by suppressing adverse energy back-transfer from  $\text{Ho}^{3+}$  to  $\text{Nd}^{3+}$  with the help of the spatial separation between them.

Samples of the 20Yb/1Ho/xCe ( $x = 0, 1, 5, 10, 20$ , and 30 mol %):  $\text{NaGdF}_4$  core NCs, 20Yb/1Ho/10Ce:  $\text{NaGdF}_4@\text{NaYF}_4$  active-core@inert-shell NCs and 20Yb/1Ho/xCe:  $\text{NaGdF}_4@\text{20Yb}/\text{yNd}$  ( $y = 0.1, 0.5, 1, 5, 10$  and 20):  $\text{NaYF}_4$  active-core@active-shell NCs were synthesized by a coprecipitation method. X-ray diffraction (XRD) patterns of two typical core and core–shell products are shown in Supporting Information Figure S1. All the XRD peaks of the core and core–shell samples can be well indexed by the standard pattern of the hexagonal phase  $\beta\text{-NaGdF}_4$  (JCPDS. No. 27-0699). It is observed that the diffraction peaks tend to be sharpened from the core to core–shell, verifying an increase in the mean grain size after growing shell on the surface of core. Transmission electron microscopy (TEM) images, shown in Figure 1a and Supporting Information Figure S2, demonstrate that the nanoparticles are monodispersed with the mean sizes of  $\sim 10$  nm and  $\sim 50$  nm (diameter)  $\times \sim 22$  nm (length, along  $c$  axis) for core and core–shell NCs, respectively. The selected area electron diffraction (SAED) pattern (inset of Figure 1a) of the core–shell NCs confirms that they are pure hexagonal phase. High-resolution TEM (HRTEM) image for an individual core–shell NC (Figure 1c) and the corresponding SAED pattern (Figure 1d) reveal its single-crystalline nature with high-crystallinity. The lattice fringes are clearly resolved, and a typical  $d$ -spacing around 0.52 nm is observed, corresponding to the (100) plane of hexagonal  $\text{NaGdF}_4$  phase (Figure 1c). High-angle annular dark-field (HAADF) scanning TEM (STEM) observation, which is sensitive to the atomic number ( $Z$ ) difference in the sample, is adopted to characterize the 20Yb/1Ho/30Ce:  $\text{NaGdF}_4@\text{20Yb}/\text{20Nd}: \text{NaYF}_4$  core–shell NCs. As shown in Figure 1b, owing to the large difference of atomic number between Gd ( $Z = 64$ ) and Y ( $Z = 39$ ), the obvious contrast for the core (bright) and the outer shell (dark) is clearly observed, confirming the successful formation of core–shell nanoarchitecture with shell completely covering on core. Evidently, EDS elemental mappings, performed on an individual 20Yb/1Ho/30Ce:  $\text{NaGdF}_4@\text{20Yb}/\text{20Nd}: \text{NaYF}_4$  core–shell NC, verify Gd/Ce in the core, Y/Nd locating in the shell, and Yb crossing from the core to the shell.

Under the excitation of 980 nm laser,  $\text{Ce}^{3+}$  doping-dependent UC luminescent behaviors of 20Yb/1Ho/xCe ( $x = 0, 1, 5, 10, 20$ , and 30 mol %):  $\text{NaGdF}_4$  core NCs are

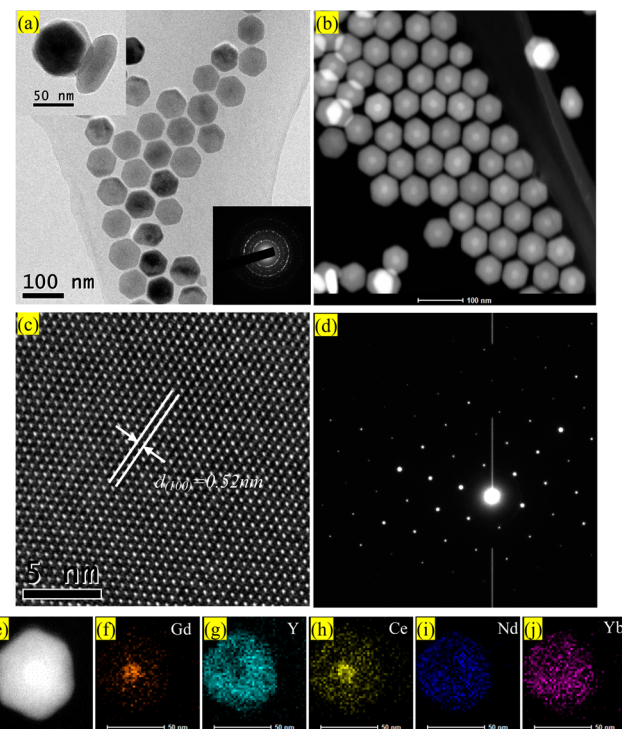


**Figure 1.** (a) TEM and (b) HAADF-STEM micrographs of (a) 20Yb/1Ho/30Ce:  $\text{NaGdF}_4@\text{20Yb}/\text{20Nd}: \text{NaYF}_4$  core–shell NCs. Insets of (a) show the SAED pattern of these core–shell NCs (bottom) and the enlarged core–shell NCs (top). (c, d) are HRTEM image for an individual NC and the corresponding SAED pattern. (e–j) STEM-HAADF image of an individual 20Yb/1Ho/30Ce:  $\text{NaGdF}_4@\text{20Yb}/\text{20Nd}: \text{NaYF}_4$  core–shell NC with associated Gd, Y, Ce, Nd, and Yb elemental mapping.

investigated. All the UC spectra show emission bands centered at 541 (green), 648 (red), and 750 nm (NIR) originated from  $\text{Ho}^{3+}\text{:}^5\text{S}_2, ^5\text{F}_4 \rightarrow {}^5\text{I}_8$ ,  ${}^5\text{F}_5 \rightarrow {}^5\text{I}_8$ , and  ${}^5\text{S}_2, ^5\text{F}_4 \rightarrow {}^5\text{I}_7$  transitions, respectively (Figure 2a).  $\text{Ce}^{3+}$  doping is found to be beneficial for the UC color tuning from green to red in the present core NCs (Figure 2b). Increasing  $\text{Ce}^{3+}$  dopants will result in monotonous enhancement of red to green UC intensity ratio of  $\text{Ho}^{3+}$ , which is clearly demonstrated by the change of luminescent photographs as well as color coordinates in the Commission International de l'Eclairage (CIE) 1931 chromaticity diagram (Figure 2c). Importantly, when  $\text{Ce}^{3+}$  content is higher than 10 mol %, pure red UC luminescence is easily achieved. Furthermore, the integrated UC intensity is found to monotonously decrease with increase of  $\text{Ce}^{3+}$  content, as demonstrated in Figure 2b, which is attributed to the depopulation of electrons in green-emitting  ${}^5\text{S}_2, {}^5\text{F}_4$  states and red-emitting  ${}^5\text{F}_5$  one of  $\text{Ho}^{3+}$  via a cross relaxation between  $\text{Ho}^{3+}$  and  $\text{Ce}^{3+}$  and will be discussed in detailed in the following section. Using the similar method reported by Chen and Prasad et al. (see the Experimental Methods),<sup>28,29</sup> the UC efficiencies of the Yb/Ho (20/1 mol %):  $\text{NaGdF}_4$  and Yb/Ho/Ce (20/1/30 mol %):  $\text{NaGdF}_4$  core NCs are roughly estimated to be 0.007% and 0.004% with the excitation power density of 20 W/cm<sup>2</sup>, respectively.

For both Yb/Ho codoped and Yb/Ho/Ce triply doped core samples, the power-dependent UC emission spectra have been recorded (not provided here), which gives the quadratic dependence of red or green UC intensity on the pumping power. This result reveals that the electron population in the

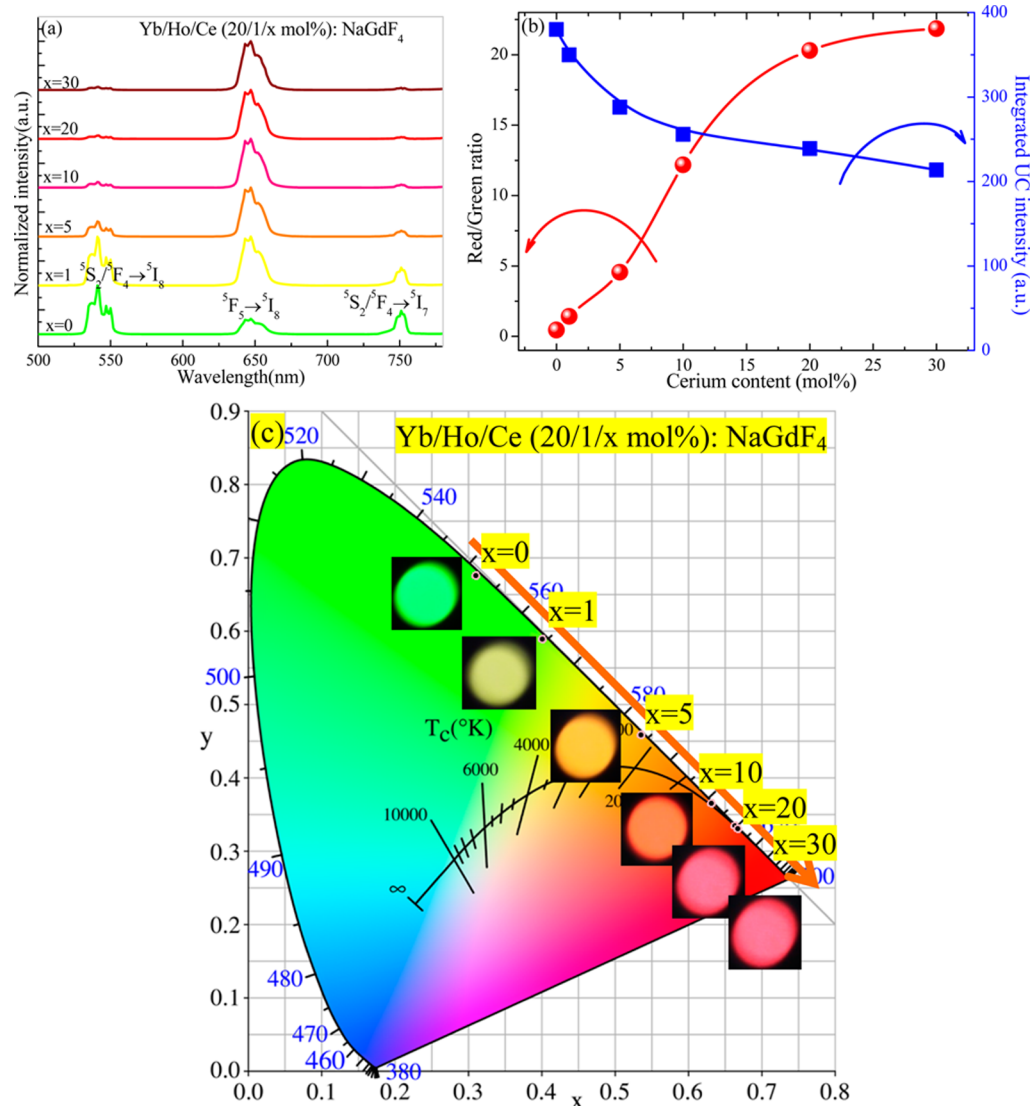


**Figure 2.** (a) Ce<sup>3+</sup> content-dependent UC emission spectra for Yb/Ho/Ce: NaGdF<sub>4</sub> core NCs; (b) the integrated UC intensity as well as the ratio of red to green emission versus Ce<sup>3+</sup> content; (c) Ce<sup>3+</sup> content-dependent color coordinates of Yb/Ho/Ce: NaGdF<sub>4</sub> core NCs in CIE chromaticity diagram; the corresponding UC luminescent images are also provided in the inset of (c).

<sup>5</sup>F<sub>5</sub> and <sup>5</sup>S<sub>2</sub>, <sup>5</sup>F<sub>4</sub> states of Ho<sup>3+</sup> is a two-photon UC process. Under 980 nm laser excitation, Yb<sup>3+</sup> sensitizers are activated from <sup>2</sup>F<sub>7/2</sub> ground state to <sup>2</sup>F<sub>5/2</sub> excited state via ground state absorption (GSA). Afterward, the <sup>5</sup>I<sub>6</sub> and <sup>5</sup>S<sub>2</sub>, <sup>5</sup>F<sub>4</sub> states of Ho<sup>3+</sup> are populated through ETs from Yb<sup>3+</sup> to Ho<sup>3+</sup>, which induces green and NIR UC emissions ascribing to Ho<sup>3+</sup><sup>5</sup>S<sub>2</sub>, <sup>5</sup>F<sub>4</sub> → <sup>5</sup>I<sub>8</sub> and <sup>5</sup>S<sub>2</sub>, <sup>5</sup>F<sub>4</sub> → <sup>5</sup>I<sub>7</sub> transitions, respectively. The population of <sup>5</sup>F<sub>5</sub> state of Ho<sup>3+</sup> is realized via nonradiative deactivation of <sup>5</sup>S<sub>2</sub>, <sup>5</sup>F<sub>4</sub> states or ET process of Ho<sup>3+</sup>: <sup>5</sup>I<sub>7</sub> + Yb<sup>3+</sup>: <sup>2</sup>F<sub>5/2</sub> → Ho<sup>3+</sup>: <sup>5</sup>F<sub>5</sub> + Yb<sup>3+</sup>: <sup>2</sup>F<sub>7/2</sub>. Notably, the maximum phonon energy of NaGdF<sub>4</sub> crystal is about 370 cm<sup>-1</sup>.<sup>30</sup> As a consequence, eight and nine phonons are required to bridge the energy gaps between <sup>5</sup>S<sub>2</sub> and <sup>5</sup>F<sub>5</sub> (3000 cm<sup>-1</sup>) as well as between <sup>5</sup>I<sub>6</sub> and <sup>5</sup>I<sub>7</sub> (3400 cm<sup>-1</sup>), respectively, and subsequently, the nonradiative relaxation probability from <sup>5</sup>S<sub>2</sub> and <sup>5</sup>I<sub>6</sub> states to the lower ones is quite low, which results in the low red to green UC emission ratio in the Yb/Ho: NaGdF<sub>4</sub> sample (without Ce<sup>3+</sup> doping), as evidenced in Figure 1a.

Upon introducing Ce<sup>3+</sup> dopants into Yb/Ho: NaGdF<sub>4</sub>, the red to green ratio significantly increases (Figure 2a,b), revealing

that Ce<sup>3+</sup> ions play a key role for enhancing Ho<sup>3+</sup> red UC emission and weakening green one. To reveal the ET interactions between Ce<sup>3+</sup> and Ho<sup>3+</sup>, Ce<sup>3+</sup> doping-dependent UC decay curves of Ho<sup>3+</sup><sup>5</sup>S<sub>2</sub>, <sup>5</sup>F<sub>4</sub>, and <sup>5</sup>F<sub>5</sub> states and photoluminescence decay profiles of Ho<sup>3+</sup><sup>5</sup>I<sub>6</sub> one in the Yb/Ho/Ce: NaGdF<sub>4</sub> NCs were recorded under 980 NIR laser excitation, as shown in Figure 3a–c and tabulated in Table 1. Because of the nonsingle-exponential feature of these decay curves, the decay lifetime was evaluated based on the following equation:<sup>31</sup>

$$\tau_{\text{exp}} = \int I(t) dt / I_p \quad (1)$$

where  $I_p$  is the peak intensity in the decay curve, and  $I(t)$  the time-dependent UC emission intensity. With increase of Ce<sup>3+</sup> doping content, the gradual decrease for the lifetimes of the green-emitting <sup>5</sup>S<sub>2</sub>, <sup>5</sup>F<sub>4</sub> states, the intermediate state <sup>5</sup>I<sub>6</sub> as well as the red-emitting <sup>5</sup>F<sub>5</sub> one of Ho<sup>3+</sup> clearly evidence the occurrence of energy transfer from Ho<sup>3+</sup> to Ce<sup>3+</sup>. Importantly, compared to the cases of the <sup>5</sup>S<sub>2</sub>, <sup>5</sup>F<sub>4</sub>, and <sup>5</sup>I<sub>6</sub> states, the lifetime for the <sup>5</sup>F<sub>5</sub> state is not greatly affected by Ce<sup>3+</sup> doping, i.e., the

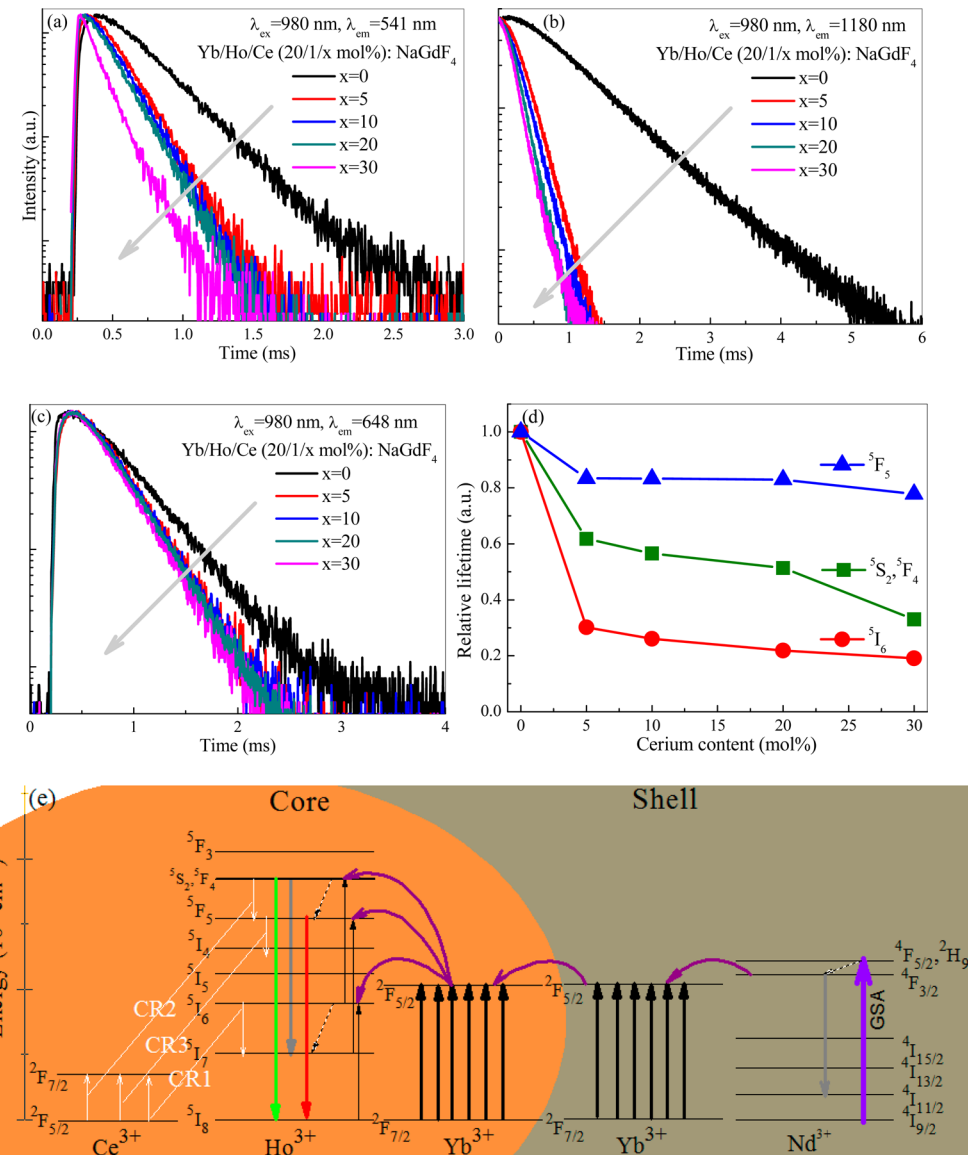


**Figure 3.** Ce<sup>3+</sup> doping-dependent decay curves of (a) Ho<sup>3+</sup>:<sup>5</sup>S<sub>2</sub>,<sup>5</sup>F<sub>4</sub>, (b) <sup>5</sup>I<sub>6</sub>, and (c) <sup>5</sup>F<sub>5</sub> states in Yb/Ho/Ce: NaGdF<sub>4</sub> core NCs under 980 nm laser excitation. (d) Corresponding relative lifetimes of these excited states versus Ce<sup>3+</sup> content. (e) Energy level diagrams of Ce<sup>3+</sup>, Ho<sup>3+</sup>, Yb<sup>3+</sup>, and Nd<sup>3+</sup> as well as the proposed mechanisms for the achievement of pure red UC luminescence under 980 or 808 nm laser excitation in Yb/Ho/Ce: NaGdF<sub>4</sub>@Yb/Nd: NaYF<sub>4</sub> core–shell NCs.

**Table 1. Dependence of Lifetimes and Energy Transfer Efficiency, ETE, on Ce<sup>3+</sup> Doping Content for Ho<sup>3+</sup>:<sup>5</sup>S<sub>2</sub>,<sup>5</sup>F<sub>4</sub>, <sup>5</sup>I<sub>6</sub>, and <sup>5</sup>F<sub>5</sub> States in Yb/Ho/Ce (20/1/x Mol %): NaGdF<sub>4</sub> Core NCs**

sample	<sup>5</sup> S <sub>2</sub> , <sup>5</sup> F <sub>4</sub> (μs)	ETE (%)	<sup>5</sup> I <sub>6</sub> (μs)	ETE (%)	<sup>5</sup> F <sub>5</sub> (μs)	ETE (%)
x = 0	518		1281		658	
x = 5	320	38.2	387	69.8	549	16.6
x = 10	293	43.4	334	73.9	548	16.7
x = 20	256	50.6	280	78.1	546	17.0
x = 30	171	67.0	245	80.9	512	22.2

decrease of lifetime for the <sup>5</sup>F<sub>5</sub> state is far slower than that for the <sup>5</sup>S<sub>2</sub>,<sup>5</sup>F<sub>4</sub>, and <sup>5</sup>I<sub>6</sub> states (Figure 3d). Figure 3e shows energy levels of Ce<sup>3+</sup>, Ho<sup>3+</sup>, and Yb<sup>3+</sup> ions as well as the proposed mechanisms to explain the realization of single-band red UC emission in Yb/Ho/Ce: NaGdF<sub>4</sub> core NCs. According to the above-mentioned lifetime results as well as energy match

conditions, three cross-relaxation (CR) processes involving Ce<sup>3+</sup> and Ho<sup>3+</sup>, that is, CR1: Ho<sup>3+</sup>:<sup>5</sup>I<sub>6</sub> + Ce<sup>3+</sup>:<sup>2</sup>F<sub>5/2</sub> → Ho<sup>3+</sup>:<sup>5</sup>I<sub>7</sub> + Ce<sup>3+</sup>:<sup>2</sup>F<sub>7/2</sub>, CR2: Ho<sup>3+</sup>:<sup>5</sup>S<sub>2</sub>,<sup>5</sup>F<sub>4</sub> + Ce<sup>3+</sup>:<sup>2</sup>F<sub>5/2</sub> → Ho<sup>3+</sup>:<sup>5</sup>F<sub>5</sub> + Ce<sup>3+</sup>:<sup>2</sup>F<sub>7/2</sub> and CR3: Ho<sup>3+</sup>:<sup>5</sup>F<sub>5</sub> + Ce<sup>3+</sup>:<sup>2</sup>F<sub>5/2</sub> → Ho<sup>3+</sup>:<sup>5</sup>I<sub>4</sub> + Ce<sup>3+</sup>:<sup>2</sup>F<sub>7/2</sub>, were proposed to explain the observed phenomena. The CR1 and CR2 processes are beneficial to depopulating the electrons in the green-emitting <sup>5</sup>S<sub>2</sub>,<sup>5</sup>F<sub>4</sub> state and its intermediate <sup>5</sup>I<sub>6</sub> one while populating the red-emitting <sup>5</sup>F<sub>5</sub> state and its intermediate state <sup>5</sup>I<sub>7</sub> one.<sup>25</sup> On the other hand, the CR3 process is harmful for red UC luminescence by depopulating <sup>5</sup>F<sub>5</sub> state. Based on the decay lifetime, the energy transfer efficiencies (ETEs) of the CR1, CR2 and CR3 processes can be calculated by the following expression:<sup>32</sup>

$$\eta_{\text{ETE}} = 1 - \frac{\tau_{\text{Yb/Ho/Ce}}}{\tau_{\text{Yb/Ho}}} \quad (2)$$

where  $\tau_{\text{Yb/Ho}}$  and  $\tau_{\text{Yb/Ho/Ce}}$  are the lifetimes of Ho<sup>3+</sup> in the Yb/Ho codoped and Yb/Ho/Ce triply doped samples, respectively.

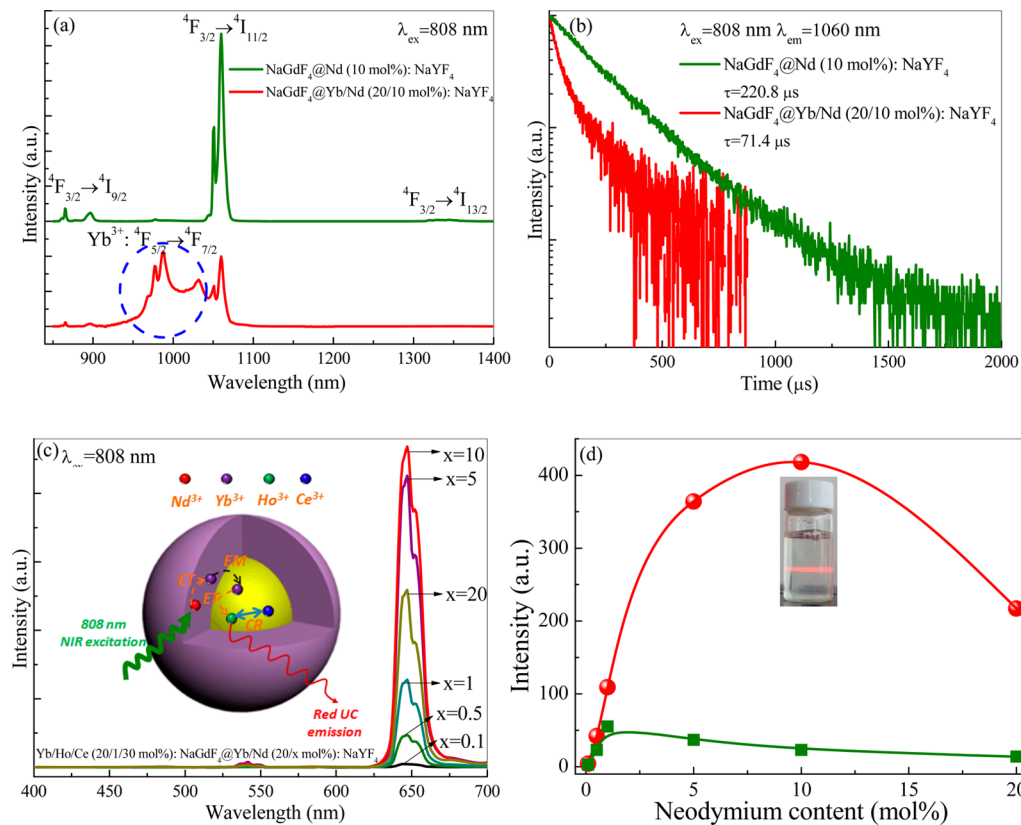


**Figure 4.** (a) Photoluminescence spectra of  $\text{NaGdF}_4@\text{Nd:NaYF}_4$  and  $\text{NaGdF}_4@\text{Yb/Nd:NaYF}_4$  core–shell NCs. (b) Decay curves of  $\text{Nd}^{3+}:{}^4\text{F}_{3/2}$  state in these two corresponding samples. (c)  $\text{Nd}^{3+}$ -content dependence of UC emission spectra of  $\text{Yb/Ho/Ce}$  (20/1/30 mol %):  $\text{NaGdF}_4@\text{Yb/Nd}$  ( $20/x$  mol %):  $\text{NaYF}_4$  active-core@active-shell NCs under 808 nm laser excitation (the excitation power density:  $20 \text{ W/cm}^2$ ); inset shows the schematic active-core@active-shell structure and the related energy transfer processes. (d) Integrated UC emission intensity versus  $\text{Nd}^{3+}$  doping content for  $\text{Yb/Ho/Ce: NaGdF}_4@\text{Yb/Nd: NaYF}_4$  active-core@active-shell NCs (red ●) and  $\text{Yb/Ho/Ce/Nd: NaGdF}_4@\text{Yb/Nd: NaYF}_4$  active-core@inert-shell NCs (green ■), respectively. Inset is UC luminescent photograph of  $\text{Yb/Ho/Ce: NaGdF}_4@\text{Yb/Nd: NaYF}_4$  NCs (1 wt %) dispersed in cyclohexane under 808 nm laser excitation ( $20 \text{ W/cm}^2$ ).

As evidenced in Table 1, the ETEs of CR1 and CR2 processes reach as high as 80.9% and 67.0%, respectively, whereas that of CR3 is only 22.2% for  $\text{Ce}^{3+}$  doping content as high as 30 mol %. This result illustrates that the CR1 and CR2 processes are far more efficient than that of CR3 one, being beneficial to the realization of single-band red UC radiation of  $\text{Ho}^{3+}$  by simply modifying  $\text{Ce}^{3+}$  dopants.

In a further work, UC emission spectra and decay curves of the  $\text{Yb/Ho/Ce: NaGdF}_4$  core and  $\text{Yb/Ho/Ce: NaGdF}_4@\text{NaYF}_4$  active-core@inert-shell NCs were recorded to illustrate the impact of core–shell structure on optical performance, as provided in Supporting Information Figure S3. Obviously, significant enhancement (about 10 times) in overall emission intensity is found after growth of  $\text{NaYF}_4$  inert-shell on the  $\text{Yb/Ho/Ce: NaGdF}_4$  core (Supporting Information Figure S3a). As evidenced in Supporting Information Figure S3b and c, the slower UC decays for the  ${}^5\text{S}_2$ ,  ${}^5\text{F}_4$ , and  ${}^5\text{F}_5$  states of  $\text{Ho}^{3+}$  in core–shell NCs than those in core-only ones clearly confirm the surface passivation role of shell. Generally, the core–shell nanoarchitecture differs from the core in removing the surface effect. This difference might be understood as follows: the core–shell structure separates in space from the surface for the luminescent activators, which can (i) block the excitation energy transportation to surface quenching centers to a certain extent and (ii) recover the surface luminescent centers that are severely quenched in the core.<sup>33</sup> Moreover, the multiphonon relaxation processes in the luminescent centers mediated by the

surface-related organic high vibrational frequency modes will be different: the core–shell structure lengthens the distance between the luminescent centers and the vibrational modes, which will dim the interaction between them and, thus, cause the nonradiative vibrational relaxation processes to be less efficient compared to the core sample.

Finally,  $\text{Yb/Ho/Ce: NaGdF}_4@\text{Yb/Nd: NaYF}_4$  active-core@active-shell NCs were prepared to investigate their UC performance under 808 nm laser excitation (corresponding to  ${}^4\text{I}_{9/2} \rightarrow {}^4\text{F}_{5/2}, {}^2\text{H}_{9/2}$  absorption transition of  $\text{Nd}^{3+}$ ). First, photoluminescence spectra and decay behaviors of  $\text{NaGdF}_4@\text{Nd}$  (10 mol %):  $\text{NaYF}_4$  and  $\text{NaGdF}_4@\text{Yb/Nd}$  (20/10 mol %):  $\text{NaYF}_4$  core–shell NCs were recorded to study the energy transfer process between  $\text{Nd}^{3+}$  and  $\text{Yb}^{3+}$ . As shown in Figure 4a, several emission bands in the NIR region, assigned to the  ${}^4\text{F}_{3/2} \rightarrow {}^4\text{I}_{9/2}$  (872 nm),  ${}^4\text{F}_{3/2} \rightarrow {}^4\text{I}_{11/2}$  (1060 nm), and  ${}^4\text{F}_{3/2} \rightarrow {}^4\text{I}_{13/2}$  (1345 nm) transitions of  $\text{Nd}^{3+}$ , are observed in the  $\text{Nd}^{3+}$  single-doped product under 808 nm laser excitation. After introducing  $\text{Yb}^{3+}$  into the sample, all the  $\text{Nd}^{3+}$  emission-band intensities are significantly depressed, whereas an intense NIR emission at about 980 nm ascribing to the  $\text{Yb}^{3+}: {}^2\text{F}_{5/2} \rightarrow {}^2\text{F}_{7/2}$  transition emerges in the  $\text{Nd}^{3+}/\text{Yb}^{3+}$  codoped core–shell NCs, indicating the existence of energy transfer from  $\text{Nd}^{3+}$  and  $\text{Yb}^{3+}$ . This is further supported by the fact that the decay lifetime of the  $\text{Nd}^{3+}: {}^4\text{F}_{3/2}$  state is remarkably shortened from 220.8 to 71.4  $\mu\text{s}$  when adding  $\text{Yb}^{3+}$  into the  $\text{Nd}^{3+}$ -doped sample (Figure 4b), owing to the introducing of the extra decay pathway, that is,

energy transfer from the  $\text{Nd}^{3+}$ :  $^4\text{F}_{3/2}$  state to the  $\text{Yb}^{3+}$ :  $^2\text{F}_{5/2}$  one via the  $\text{Nd}^{3+}$ :  $^4\text{F}_{3/2}$  +  $\text{Yb}^{3+}$ :  $^2\text{F}_{7/2}$   $\rightarrow$   $\text{Nd}^{3+}$ :  $^4\text{I}_{11/2}$  +  $\text{Yb}^{3+}$ :  $^2\text{F}_{5/2}$  process (Figure 3e). Notably, a nearly 68% efficiency is realized for energy transfer between  $\text{Nd}^{3+}$ :  $^4\text{F}_{3/2}$  and  $\text{Yb}^{3+}$ :  $^2\text{F}_{5/2}$ , confirming that the  $\text{Nd}^{3+}$  absorbers can efficiently transfer energy to  $\text{Yb}^{3+}$  sensitizers. Afterward, we studied the 808 nm excited UC behaviors of the  $\text{Yb}/\text{Ho}/\text{Ce}$ :  $\text{NaGdF}_4@\text{Yb}/\text{Nd}$ :  $\text{NaYF}_4$  NCs. As expected, such active-core@active-shell nano-architecture could be efficiently activated under 808 nm irradiation, giving rise to the characteristic red luminescence of  $\text{Ho}^{3+}$  (Figure 4c). In addition, the single-band red UC luminescence of  $\text{Ho}^{3+}$  in the present core–shell NCs is found to be independent of the excitation power density (in the range of 2–60  $\text{W}/\text{cm}^2$ ). In contrast, no noticeable  $\text{Ho}^{3+}$  emission signal (not shown here) was detected from nanoparticles without  $\text{Nd}^{3+}$  or  $\text{Yb}^{3+}$  added, for example, the  $\text{Yb}/\text{Ho}/\text{Ce}$ :  $\text{NaGdF}_4@\text{Yb}$ :  $\text{NaYF}_4$  or  $\text{Yb}/\text{Ho}/\text{Ce}$ :  $\text{NaGdF}_4@\text{Nd}$ :  $\text{NaYF}_4$  NCs. These control experiments showed that both the  $\text{Nd}^{3+}$  and  $\text{Yb}^{3+}$  ions in shell are necessary for the realization of 808 nm-excited red UC luminescence of  $\text{Ho}^{3+}$ , where  $\text{Nd}^{3+}$  ions are the efficient sensitizers to absorb 808 nm NIR laser while  $\text{Yb}^{3+}$  ions act as efficient energy migrators (or bridging centers) to facilitate energy transfer from  $\text{Nd}^{3+}$  ions to activator ions (i.e.,  $\text{Ho}^{3+}$ ). Based on the above results, the detailed energy transfer processes responsible for the achievement of 808 nm-excited red UC luminescence of  $\text{Ho}^{3+}$  in the  $\text{Yb}/\text{Ho}/\text{Ce}$ :  $\text{NaGdF}_4@\text{Yb}/\text{Nd}$ :  $\text{NaYF}_4$  core–shell NCs are proposed and schematically illustrated in Figure 3e and the inset of Figure 4c. The 808 nm pumping photons excite  $\text{Nd}^{3+}$  through  $^4\text{I}_{9/2} \rightarrow ^4\text{F}_{5/2}$  transition by ground state absorption, followed with nonradiative relaxation to the  $^4\text{F}_{3/2}$  state. The energy could transfer to nearby  $\text{Yb}^{3+}$  and populate its  $^2\text{F}_{5/2}$  state through  $\text{Nd}^{3+}$ :  $^4\text{F}_{3/2}$  +  $\text{Yb}^{3+}$ :  $^2\text{F}_{7/2} \rightarrow \text{Nd}^{3+}$ :  $^4\text{I}_{11/2}$  +  $\text{Yb}^{3+}$ :  $^2\text{F}_{5/2}$  and further transfer to nearby  $\text{Yb}^{3+}$  ions crossing the shell via energy migration to the core. This ET route would initiate a typical UC process in the core, with  $\text{Ho}^{3+}$  ions excited to high-energy states like  $^5\text{S}_2$ ,  $^5\text{F}_4$ , and  $^5\text{F}_5$ . In the end, two efficient cross-relaxation processes between  $\text{Ho}^{3+}$  and  $\text{Ce}^{3+}$ , that is,  $\text{Ho}^{3+}$ :  $^5\text{I}_6$  +  $\text{Ce}^{3+}$ :  $^2\text{F}_{5/2} \rightarrow \text{Ho}^{3+}$ :  $^5\text{I}_7$  +  $\text{Ce}^{3+}$ :  $^2\text{F}_{7/2}$  (CR1) and  $\text{Ho}^{3+}$ :  $^5\text{S}_2$ / $^5\text{F}_4$  +  $\text{Ce}^{3+}$ :  $^2\text{F}_{5/2} \rightarrow \text{Ho}^{3+}$ :  $^5\text{F}_5$  +  $\text{Ce}^{3+}$ :  $^2\text{F}_{7/2}$  (CR2) in the core, greatly suppress the population of green-emitting  $^5\text{S}_2$ ,  $^5\text{F}_4$  state and enhance the population of red-emitting  $^5\text{F}_5$  one, leading to bright pure red UC radiation of  $\text{Ho}^{3+}$ .

We next carried out experiments to optimize the doping content of  $\text{Nd}^{3+}$  sensitizers in the shell for the  $\text{Yb}/\text{Ho}/\text{Ce}$  (20/1/30 mol %):  $\text{NaGdF}_4@\text{Yb}/\text{Nd}$  (20/ $x$  mol %):  $\text{NaYF}_4$  active-core@active-shell NCs, as shown in Figure 4d. It is found that the optimal  $\text{Nd}^{3+}$  concentration for efficient 808 nm excited red UC luminescence is 10 mol %. As a comparison, when  $\text{Nd}^{3+}$  ions were incorporated into the core for the  $\text{Yb}/\text{Ho}/\text{Ce}/\text{Nd}$  (20/1/30/ $x$  mol %):  $\text{NaGdF}_4@\text{NaYF}_4$  active-core@inert-shell NCs, the strongest luminescence occurs only with a very low  $\text{Nd}^{3+}$  content of 1 mol % (Figure 4d). Although higher  $\text{Nd}^{3+}$  contents are favorable for sensitization, the high doping level could inevitably result in the harsh quenching effect mainly caused by efficient energy back-transfer from activators to  $^4\text{I}_J$  manifolds of  $\text{Nd}^{3+}$ .<sup>19</sup> Therefore, the doping content of  $\text{Nd}^{3+}$  in the  $\text{Yb}/\text{Ho}/\text{Ce}/\text{Nd}$ :  $\text{NaGdF}_4@\text{NaYF}_4$  NCs is restricted to a quite low level (1 mol %) to minimize quenching interactions. However, with the help of the active-shell design, where  $\text{Nd}^{3+}$  ions were doped in the shell, the adverse energy back-transfer from  $\text{Ho}^{3+}$  to  $\text{Nd}^{3+}$  is highly suppressed due to the spatial separation and large ionic distance between them and, thus, an

elevated amount of  $\text{Nd}^{3+}$  (10 mol %) in the NCs is beneficial to the realization of the improved red UC luminescence of  $\text{Ho}^{3+}$  activators. For example, the integrated emission intensity of the  $\text{Yb}/\text{Ho}/\text{Ce}$ :  $\text{NaGdF}_4@\text{Yb}/\text{Nd}$ :  $\text{NaYF}_4$  active-core@inert–shell NCs with 10 mol %  $\text{Nd}^{3+}$  in the shell layer is about 20 times as high as that of the  $\text{Yb}/\text{Ho}/\text{Ce}/\text{Nd}$ :  $\text{NaGdF}_4@\text{NaYF}_4$  active-core@inert–shell NCs with the same content of  $\text{Nd}^{3+}$  in the core (Figure 4d). The UC efficiency of the  $\text{Yb}/\text{Ho}/\text{Ce}$  (20/1/30 mol %):  $\text{NaGdF}_4@\text{Yb}/\text{Nd}$  (20/10 mol %):  $\text{NaYF}_4$  core–shell NCs is determined to be 0.052% with the excitation power density of 20  $\text{W}/\text{cm}^2$ . Apparently, the 808 nm excited  $\text{Ho}^{3+}$  red UC luminescence in the  $\text{Nd}^{3+}$ -sensitized active-core@active–shell NCs could be easily visible by the naked eyes, as exhibited in the inset of Figure 4d.

In summary, we have developed a new type of UCNCs based on the elaborate combination of  $\text{Nd}^{3+}$  sensitization,  $\text{Ce}^{3+}$ -assisted cross-relaxation and the active-core@active-shell structure design that exhibit intense single-band red luminescence of  $\text{Ho}^{3+}$  upon excitation of 808 nm. The usage of  $\text{Nd}^{3+}$  ions as sensitizers facilitates the energy transfer and photon UC of  $\text{Ho}^{3+}$  activators at a biocompatible excitation wavelength (808 nm), which will significantly minimize the overheating problem associated with conventional 980 nm excitation. The doping of  $\text{Ce}^{3+}$  plays a key role in the realization of  $\text{Ho}^{3+}$  single-band red luminescence via the efficient cross relaxation processes between  $\text{Ce}^{3+}$  and  $\text{Ho}^{3+}$ , that is,  $\text{Ho}^{3+}$ :  $^5\text{S}_2$ / $^5\text{F}_4$  +  $\text{Ce}^{3+}$ :  $^2\text{F}_{5/2} \rightarrow \text{Ho}^{3+}$ :  $^5\text{F}_5$  +  $\text{Ce}^{3+}$ :  $^2\text{F}_{7/2}$  and  $\text{Ho}^{3+}$ :  $^5\text{I}_6$  +  $\text{Ce}^{3+}$ :  $^2\text{F}_{5/2} \rightarrow \text{Ho}^{3+}$ :  $^5\text{I}_7$  +  $\text{Ce}^{3+}$ :  $^2\text{F}_{7/2}$ . The design of core–shell nanoarchitecture enables the spatial separation between  $\text{Ho}^{3+}$  and  $\text{Nd}^{3+}$  and subsequently the high-content  $\text{Nd}^{3+}$  doping to efficiently improve UC luminescence, which might finally provide highly attractive luminescent biomarkers for bioimaging without concern of overheating effect.

## EXPERIMENTAL METHODS

**Materials.** All the raw materials, including gadolinium chloride ( $\text{GdCl}_3 \cdot 6\text{H}_2\text{O}$ , 99.9%), yttrium chloride ( $\text{YCl}_3 \cdot 6\text{H}_2\text{O}$ , 99.9%), ytterbium chloride ( $\text{YbCl}_3 \cdot 6\text{H}_2\text{O}$ , 99.9%), holmium chloride ( $\text{HoCl}_3 \cdot 6\text{H}_2\text{O}$ , 99.9%), cerium chloride ( $\text{CeCl}_3 \cdot 6\text{H}_2\text{O}$ , 99.9%), neodymium chloride ( $\text{NdCl}_3 \cdot 6\text{H}_2\text{O}$ , 99.9%), ammonium fluoride ( $\text{NH}_4\text{F}$ , 99%), sodium hydroxide ( $\text{NaOH}$ , 99%), oleic acid (OA, 90%), and 1-octadecene (ODE, 90%), were purchased from Sinopharm Chemical Reagent Company and were directly used without further refinement.

**Synthesis.** The core and core–shell NCs were fabricated by a coprecipitate method. Taking  $\text{Yb}/\text{Ho}/\text{Ce}$  (20/1/30 mol %):  $\text{NaGdF}_4@\text{Yb}/\text{Nd}$  (20/10 mol %):  $\text{NaYF}_4$  core–shell nano-architecture as a typical example, a total amount of 0.8 mmol rare earth chlorides, including  $\text{GdCl}_3 \cdot 6\text{H}_2\text{O}$  (0.392 mmol),  $\text{YbCl}_3 \cdot 6\text{H}_2\text{O}$  (0.16 mmol),  $\text{HoCl}_3 \cdot 6\text{H}_2\text{O}$  (0.008 mmol), and  $\text{CeCl}_3 \cdot 6\text{H}_2\text{O}$  (0.24 mmol), were first dissolved in 1 mL of deionized water. Afterward, this rare earth aqueous solution was mixed with 8 mL of OA in a 100 mL three-necked bottle and was heated at 150 °C for 30 min to remove water. Then 12 mL of ODE was introduced into the bottle quickly to form a clear solution with another 30 min heating and subsequently cooled to room temperature naturally. Afterward, 3 mmol of  $\text{NH}_4\text{F}$  and 2 mmol of  $\text{NaOH}$  dissolved in 10 mL of methanol were added to the resulted solution with stirring at 50 °C for 30 min to evaporate the methanol. Finally, the temperature was elevated to 280 °C under  $\text{N}_2$  and hold for 90 min to induce the nucleation and growth of core NCs. The as-prepared cores were precipitated with the help of ethanol and redispersed in 6

mL of cyclohexane. The procedure for the growth of shell on core is similar to the case of core and is simply described as follows. First, 1 mL of aqueous solution of 1.6 mmol rare earth chlorides, including  $\text{YCl}_3 \cdot 6\text{H}_2\text{O}$  (1.12 mmol),  $\text{YbCl}_3 \cdot 6\text{H}_2\text{O}$  (0.32 mmol), and  $\text{NdCl}_3 \cdot 6\text{H}_2\text{O}$  (0.16 mmol), was added to a 100 mL three-necked bottle containing OA (8 mL) and ODE (12 mL). A clear solution was obtained after heating at 150 °C for 1 h, and then cooled down to 80 °C. Thereafter, 1 mL of cyclohexane solution of the preprepared Yb/Ho/Ce: NaGdF<sub>4</sub> core NCs was introduced to the above solution, together with 6 mmol of NH<sub>4</sub>F and 4 mmol of NaOH dissolved in 10 mL of methanol solution. After the evaporation of cyclohexane and methanol, the temperature was finally elevated to 280 °C under N<sub>2</sub> and hold for 3 h to obtain core–shell nanoarchitecture. Notably, other core–shell NCs mentioned in this study were also prepared by the similar experimental procedure.

**Characterization.** The microstructure observation of the core and core–shell NCs was performed on a JEOL JEM-2010 transmission electron microscope operated at 200 kV accelerating voltage. High-resolution TEM images and elemental mapping were carried out on an FEI aberration-corrected Titan Cubed S-Twin transmission electron microscope. XRD patterns were recorded on a DMAX2500 RIGAKU powder diffractometer using Cu K $\alpha$  radiation ( $\lambda = 1.54 \text{ \AA}$ ). Luminescence spectra were collected on an Edinburgh Instruments FSS spectrofluorometer equipped with the xenon lamp (150 W) as well as the adjustable 980 and 808 nm diode lasers as the excitation sources. Ho<sup>3+</sup> UC and Nd<sup>3+</sup> fluorescence decay curves were measured on an Edinburgh FSP920-C phosphorescence lifetime spectrometer using a tunable OPOTEK Vibrant 355II OPO pulse laser as the excitation source. Similar to the cases previously reported by Chen and Prasad et al.,<sup>28,29</sup> Ho<sup>3+</sup> UC efficiencies were roughly evaluated by a comparison method using the well-known Yb<sup>3+</sup>/Er<sup>3+</sup>:NaYF<sub>4</sub> microcrystalline powder as the reference. With the help of the integrated sphere, the UC emission spectra of the Yb<sup>3+</sup>/Er<sup>3+</sup>:NaYF<sub>4</sub> reference powder and the investigated NCs were recorded under the identical measuring condition. Based on the previous UC values of Yb<sup>3+</sup>/Er<sup>3+</sup>:NaYF<sub>4</sub>,<sup>34</sup> the UC efficiencies of the core and core–shell NCs can be accordingly determined.

## ■ ASSOCIATED CONTENT

### Supporting Information

XRD patterns, TEM/HRTEM images, UC emission spectra, and UC decay curves for the core-only and core–shell NCs. The Supporting Information is available free of charge on the ACS Publications website at DOI: 10.1021/acs.jpcllett.5b01180.

## ■ AUTHOR INFORMATION

### Corresponding Author

\*E-Mail: dqchen@hdu.edu.cn

### Notes

The authors declare no competing financial interest.

## ■ ACKNOWLEDGMENTS

This work was supported by the 151 talent's projects in the second level of Zhejiang Province, the Natural Science Foundation of Zhejiang for Distinguished Young Scholars (LR15E020001), and National Natural Science Foundation of China (21271170, 61372025).

## ■ REFERENCES

- Zhang, Y. H.; Zhang, L. X.; Deng, R. R.; Tian, J.; Zong, Y.; Jin, D. Y.; Liu, X. G. Multicolor Barcoding in a Single Upconversion Crystal. *J. Am. Chem. Soc.* **2014**, *136*, 4893–4896.
- Dong, H.; Sun, L. D.; Yan, C. H. Energy Transfer in Lanthanide Upconversion Studies for Extended Optical Applications. *Chem. Soc. Rev.* **2015**, *44*, 1608–1643.
- Chen, G. Y.; Ågren, H.; Ohulchanskyy, T. Y.; Prasad, P. N. Light Upconversion Core-Shell Nanostructures: NanoPhotonic Control for Emerging Applications. *Chem. Soc. Rev.* **2015**, *44*, 1680–1713.
- Chan, E. M. Combinatorial Approaches for Developing Upconverting Nanomaterials: High-Throughput Screening, Modelling, and Applications. *Chem. Soc. Rev.* **2015**, *44*, 1653–1679.
- Li, X. M.; Zhang, F.; Zhao, D. Y. Lab on Upconversion Nanoparticles: Optical Properties and Applications Engineering via Designed Nanostructure. *Chem. Soc. Rev.* **2015**, *44*, 1346–1378.
- Yang, D. M.; Ma, P. A.; Hou, Z. Y.; Cheng, Z. Y.; Li, C. X.; Lin, J. Current Advances in Lanthanide Ion ( $\text{Ln}^{3+}$ )-Based Upconversion Nanomaterials for Drug Delivery. *Chem. Soc. Rev.* **2015**, *44*, 1416–1448.
- Zheng, K. Z.; Qin, W. P.; Cao, C. Y.; Zhao, D.; Wang, L. NIR to VUV: Seven-Photon Upconversion Emissions from Gd<sup>3+</sup> Ions in Fluoride Nanocrystals. *J. Phys. Chem. Lett.* **2015**, *6*, 556–560.
- Hou, Z. Y.; Zhang, Y. X.; Deng, K. R.; Chen, Y. Y.; Li, X. J.; Deng, X. R.; Cheng, Z. Y.; Lian, H. Z.; Li, C. X.; Lin, J. UV-Emitting Upconversion-Based TiO<sub>2</sub> Photosensitizing Nanoplatform: Near-Infrared Light Mediated in Vivo Photodynamic Therapy via Mitochondria-Involved Apoptosis Pathway. *ACS Nano* **2015**, *9*, 2584–2599.
- Anderson, R. B.; Smith, S. J.; May, P. S.; Berry, M. T. Revisiting the NIR-Visible Upconversion Mechanism in  $\beta$ -NaYF<sub>4</sub>: Yb<sup>3+</sup>, Er<sup>3+</sup>. *J. Phys. Chem. Lett.* **2014**, *5*, 36–42.
- Wang, F.; Liu, X. G. Upconversion Multicolor Fine-Tuning: Visible to Near-Infrared Emission from Lanthanide-Doped NaYF<sub>4</sub> Nanoparticles. *J. Am. Chem. Soc.* **2008**, *130*, 5642–5643.
- Zhou, J. J.; Shirahata, N.; Sun, H. T.; Ghosh, B.; Ogawara, M.; Teng, Y.; Zhou, S. F.; Sa Chu, R. G.; Fujii, M.; Qiu, J. R. Efficient Dual-Modal NIR-to-NIR Emission of Rare Earth Ions Co-doped Nanocrystals for Biological Fluorescence Imaging. *J. Phys. Chem. Lett.* **2013**, *4*, 402–408.
- Damasco, J. A.; Chen, G. Y.; Shao, W.; Ågren, H.; Huang, H. Y.; Song, W. T.; Lovell, J. F.; Prasad, P. N. Size-Tunable and Monodisperse Tm<sup>3+</sup>/Gd<sup>3+</sup>-Doped Hexagonal NaYbF<sub>4</sub> Nanoparticles with Engineered Efficient Near Infrared-to-Near Infrared Upconversion for In Vivo Imaging. *ACS Appl. Mater. Interfaces* **2014**, *6*, 13884–13893.
- Weissleder, R. A Clearer Vision for in Vivo Imaging. *Nat. Biotechnol.* **2001**, *19*, 316–317.
- Shen, J.; Chen, G. Y.; Vu, A. M.; Fan, W.; Bilsel, O. S.; Chang, C. C.; Han, G. Engineering the Upconversion Nanoparticle Excitation Wavelength: Cascade Sensitization of Tri-doped Upconversion Colloidal Nanoparticles at 800 nm. *Adv. Opt. Mater.* **2013**, *1*, 644–650.
- Wang, Y. F.; Liu, G. Y.; Sun, L. D.; Xiao, J. W.; Zhou, J. C.; Yan, C. H. Nd<sup>3+</sup>-Sensitized Upconversion Nanophosphors: Efficient in Vivo Bioimaging Probes with Minimized Heating Effect. *ACS Nano* **2013**, *7*, 7200–7206.
- Li, X. M.; Wang, R.; Zhang, F.; Zhou, L.; Shen, D. K.; Yao, C.; Zhao, D. Y. Nd<sup>3+</sup>-Sensitized Up/Down Converting Dual-Mode Nanomaterials for Efficient In-vitro and In-vivo Bioimaging Excited at 800 nm. *Sci. Rep.* **2013**, *3*, 3536.
- Xie, X. J.; Gao, N. Y.; Deng, R. R.; Sun, Q.; Xu, Q. H.; Liu, X. G. Mechanistic Investigation of Photon Upconversion in Nd<sup>3+</sup>-Sensitized Core-Shell Nanoparticles. *J. Am. Chem. Soc.* **2013**, *135*, 12608–12611.
- Wen, H. L.; Zhu, H.; Chen, X.; Hung, T. F.; Wang, B. L.; Zhu, G. Y.; Yu, S. F.; Wang, F. Upconverting Near-Infrared Light through Energy Management in Core-Shell-Shell Nanoparticles. *Angew. Chem., Int. Ed.* **2013**, *52*, 13419–13423.
- Zhong, Y. T.; Tian, G.; Gu, Z. J.; Yang, Y. J.; Gu, L.; Zhao, Y. L.; Ma, Y.; Yao, J. N. Elimination of Photon Quenching by a Transition

Layer to Fabricate a Quenching-Shield Sandwich Structure for 800 nm Excited Upconversion Luminescence of Nd<sup>3+</sup>-Sensitized Nanoparticle. *Adv. Mater.* **2014**, *26*, 2831–2837.

(20) Wang, D.; Xue, B.; Kong, X. G.; Tu, L. P.; Liu, X. M.; Zhang, Y. L.; Chang, Y. L.; Luo, Y. S.; Zhao, H. Y.; Zhang, H. 808 nm Driven Nd<sup>3+</sup>-Sensitized Upconversion Nanostructures for Photodynamic Therapy and Simultaneous Fluorescence Imaging. *Nanoscale* **2015**, *7*, 190–197.

(21) Yi, G.; Peng, Y.; Gao, Z. Strong Red-Emitting Near-Infrared-to-Visible Upconversion Fluorescent Nanoparticles. *Chem. Mater.* **2011**, *23*, 2729–2734.

(22) Chen, D. Q.; Lei, L.; Zhang, R.; Yang, A. P.; Xu, J.; Wang, Y. S. Intrinsic Single-Band Upconversion Emission in Colloidal Yb/Er(Tm): Na<sub>3</sub>Zr(Hf)F<sub>7</sub> Nanocrystals. *Chem. Commun.* **2012**, *48*, 10630–10632.

(23) Wang, J.; Deng, R. R.; MacDonald, M. A.; Chen, B. L.; Yuan, J. K.; Wang, F.; Chi, D. Z.; Andy Hor, T. S.; Zhang, P.; Liu, G. K.; et al. Enhancing Multiphoton Upconversion through Energy Clustering at Sublattice Level. *Nat. Mater.* **2014**, *13*, 157–162.

(24) Wang, J.; Wang, F.; Wang, C.; Liu, Z.; Liu, X. G. Single-Band Upconversion Emission in Lanthanide-Doped KMnF<sub>3</sub> Nanocrystals. *Angew. Chem., Int. Ed.* **2011**, *50*, 10369–10372.

(25) Chen, G. Y.; Liu, H. C.; Somesfalean, G.; Liang, H. J.; Zhang, Z. G. Upconversion Emission Tuning from Green to Red in Yb<sup>3+</sup>/Ho<sup>3+</sup>-Codoped NaYF<sub>4</sub> Nanocrystals by Tridoping with Ce<sup>3+</sup> Ions. *Nanotechnology* **2009**, *20*, 385704.

(26) Tian, G.; Gu, Z. J.; Zhou, L. J.; Yin, W. Y.; Liu, X. X.; Yan, L.; Jin, S.; Ren, W. L.; Xing, G. M.; Li, S. Y.; et al. Mn<sup>2+</sup> Dopant-Controlled Synthesis of NaYF<sub>4</sub>:Yb/Er Upconversion Nanoparticles for in Vivo Imaging and Drug Delivery. *Adv. Mater.* **2012**, *24*, 1226–1231.

(27) Gao, W.; Zheng, H.; Han, Q.; He, E.; Gao, F.; Wang, R. Enhanced Red Upconversion Luminescence by Codoping Ce<sup>3+</sup> in  $\beta$ -NaY(Gd<sub>0.4</sub>)F<sub>4</sub>:Yb<sup>3+</sup>/Ho<sup>3+</sup> Nanocrystals. *J. Mater. Chem. C* **2014**, *2*, 5327–5334.

(28) Liu, Y. S.; Tu, D. T.; Zhu, H. M.; Li, R. F.; Luo, W. Q.; Chen, X. Y. A Strategy to Achieve Efficient Dual-Mode Luminescence of Eu<sup>3+</sup> in Lanthanides Doped Multifunctional NaGdF<sub>4</sub> Nanocrystals. *Adv. Mater.* **2010**, *22*, 3266–3271.

(29) Chen, G. Y.; Ohulchanskyy, T. Y.; Kachynski, A.; Ågren, H.; Prasad, P. N. Intense Visible and Near-Infrared Upconversion Photoluminescence in Colloidal LiYF<sub>4</sub>: Er<sup>3+</sup> Nanocrystals under Excitation at 1490 nm. *ACS Nano* **2011**, *5*, 4981–4986.

(30) Aebischer, A.; Hostettler, M.; Hauser, J.; Krämer, K.; Weber, T.; Güdel, H. U.; Bürgi, H. B. Structural and Spectroscopic Characterization of Active Sites in a Family of Light-Emitting Sodium Lanthanide Tetrafluorides. *Angew. Chem., Int. Ed.* **2006**, *45*, 2802–2806.

(31) Wang, L.; Zhang, X.; Hao, Z. D.; Lou, Y. S.; Zhang, J. H.; Wang, X. J. Interionic Energy Transfer in Y<sub>3</sub>Al<sub>5</sub>O<sub>12</sub>: Ce<sup>3+</sup>, Pr<sup>3+</sup> Phosphor. *J. Appl. Phys.* **2010**, *108*, 093515.

(32) Paulose, P. I.; Jose, G.; Thomas, V.; Unnikrishnan, N. V.; Warrier, M. K. R. Sensitized Fluorescence of Ce<sup>3+</sup>/Mn<sup>2+</sup> System in Phosphate Glass. *J. Phys. Chem. Solids* **2003**, *64*, 841–846.

(33) Wang, F.; Wang, J.; Liu, X. G. Direct Evidence of a Surface Quenching Effect on Size-Dependent Luminescence of Upconversion Nanoparticles. *Angew. Chem., Int. Ed.* **2010**, *49*, 7456–7460.

(34) Page, R. H.; Schaffers, K. I.; Waide, P. A.; Tassano, J. B.; Payne, S. A.; Krupke, W. F.; Bischel, W. K. Upconversion-Pumped Luminescence Efficiency of Rare-Earth-Doped Hosts Sensitized with Trivalent Ytterbium. *J. Opt. Soc. Am. B* **1998**, *15*, 996–1008.